Volumetric 3D printing for rapid production of medicines

Lucía Rodríguez-Pombo[1], Xiaoyan Xu[2], Alejandro Seijo-Rabina[1], Jun Jie Ong[2], Carmen Alvarez-Lorenzo[1], Carlos Rial[3], Daniel Nieto García[4,*], Simon Gaisford[2,3], Abdul W. Basit[2,3,*], Alvaro Goyanes[1,2,3,*]

[1] Departamento de Farmacología, Farmacia y Tecnología Farmacéutica, I+D Farma (GI-1645), Facultad de Farmacia, and Health Research Institute of Santiago de Compostela (IDIS), Universidade de Santiago de Compostela, 15782 Santiago de Compostela, Spain

[2] Department of Pharmaceutics, UCL School of Pharmacy, University College London, 29-39 Brunswick Square, London, WC1N 1AX, UK

[3] FabRx Ltd., Henwood House, Henwood, Ashford, Kent, TN24 8DH, UK.

[4] Complex Tissue Regeneration Department, MERLIN Institute for Technology Inspired Regenerative Medicine, Universiteitssingel 40, 6229ER Maastricht, The Netherlands.

* Correspondence: a.basit@ucl.ac.uk (A.W.B.); daniel.nieto@usc.es (D.N.G); a.goyanes@fabrx.co.uk (A.G.)

Abstract

3D printing (3DP), or additive manufacturing, has been actively investigated as one of the enabling technologies for the impending era of personalized medicines. However, existing 3DP technologies do not afford the speeds required for on-demand production of medicines in fast-paced clinical settings. Volumetric printing is a novel 3DP technology that offers rapid printing speed and overcomes the geometric and surface quality limitations of layer-based vat photopolymerization techniques. Unlike previous vat photopolymerization 3DP technologies, volumetric printing cures the entire desired 3D geometry simultaneously by exploiting the threshold behavior in the photopolymerization process that arise due to oxygen-induced polymerization inhibition. In this work, for the first time, a volumetric printer was used to fabricate drug-loaded 3D printed tablets (Printlets™) within seconds. Six resin formulations were evaluated using this printer, each composed of polyethylene glycol diacrylate (PEGDA) as the crosslinking monomer, phenyl-2,4-6-trimethyl-benzoyl-phosphinate as the photoinitiator, and paracetamol as the model drug. Water or PEG300 were included as diluents in varying concentrations to facilitate drug release. Paracetamol-loaded Printlets were successfully fabricated within 17 seconds. Drug release rates could be tuned by altering the monomer-to-diluent ratio of the photosensitive resin, with a lower ratio releasing drug faster. The present work confirms the suitability of volumetric 3DP for printing drug products in a matter of seconds. Upon further optimization, this novel technology can enable rapid, on-demand fabrication of medicines and medical devices.

Keywords: Volumetric printing; vat photopolymerization; 3D holographic printing; personalized medicines; printing pharmaceuticals; 3D printed drug products

1. Introduction

Three-dimension printing (3DP), also known as additive manufacturing, is a modern manufacturing technology that enables the layer-by-layer fabrication of 3D objects according to a computer-aided design (CAD) file [1]. Numerous fields have been disrupted by its introduction, such as aerospace engineering and automotive and medical industries [2, 3]. This is often attributed to the technology's inherent versatility, unique ability to fabricate intricate designs, and cost-effectiveness compared to traditional mass manufacturing processes [4, 5]. 3DP has supported the medical industry by enabling on-demand production of medical devices and personal protection equipment [4]. By re-locating manufacturing to hospitals, medical needs can be swiftly met regardless of a severely fractured supply chain.

The model of decentralized 3DP facilities in clinical settings can also be extended to medicines [1, 6-8]. Beyond forgoing reliance on fragile supply networks, decentralized 3DP of medicines can help tackle counterfeit products that are often introduced during transit and enable on-demand fabrication of personalized medicines. These benefits, along with the growing recognition that a tailored approach towards drug dosing and delivery affords better clinical outcomes than the traditional one-size-fits-all model, have motivated considerable research in pharmaceutical 3D printing in the past 5 years [9-17]. Enthusiasm in the field has led to numerous 3DP drug-loaded pharmaceutical products, such as polypills [18-20], tablets with braille and moon patterns for visually impaired patients [21], drug-loaded intravaginal ring [22, 23], drug-loaded hearing aids [24], intrauterine device systems [25] and drug-loaded cardiovascular prosthesis [26].

According to the American Society for Testing and Materials (ASTM) International, 3DP technologies are classified into seven major categories: binder jetting, vat polymerization, powder bed fusion, material extrusion, material jetting, directed energy deposition, and sheet lamination [27]. Among these, vat polymerization affords the highest resolution, enabling the fabrication of complex micrometer-scale models. Furthermore, unlike other 3DP technologies such as material extrusion and powder bed fusion, the materials used in vat polymerization are not subjected to high temperatures, therefore making the technology better suited for thermal-labile drugs [28]. Instead, 3D objects are produced by irradiating a vat of liquid photopolymer resin with light, activating a polymerization reaction that solidifies the irradiated resin [29-31]. Vat polymerization comprises several light-based printing technologies, of which digital light processing (DLP) and stereolithography (SLA) have already been investigated for the fabrication of personalized medicines and medical devices [32-41].

Despite the precision it offers, vat polymerization is hampered by relatively slow printing speeds. This is largely derived from the iterative layer-by-layer nature of vat polymerization and every other 3DP technology [42]. Continuous liquid interface production (CLIP) 3DP, a type of vat polymerization developed by Carbon Inc., accelerates build speeds by exploiting the principle of oxygen-inhibited photopolymerization, thereby enabling the continuous curing of the photopolymer resin as the solidified 3D object is drawn out of the resin [43]. However, the technology is not readily accessible due to the high cost and complexity of the system.

Recently, a novel vat polymerization technology called volumetric 3D printing (also known as holographic printing or multi-beam additive manufacturing) was developed, promising rapid printing speeds and isotropic mechanical properties [44-46]. In volumetric printing, the entire 3D object is simultaneously created by irradiating a volume of photosensitive resin from multiple angles, as opposed to the conventional layer-by-layer process. There are two approaches to this technology: (1) tomographic reconstruction, whereby a series of 2D light patterns, computed by a Radon transform, is projected synchronously into a rotating resin container [45, 46], and (2) employing a system architecture comprising mirrors that divide a single light beam into three orthogonal beams, projecting a holographic figure into a photosensitive resin to generate the desired object [44]. Through the superposition of multiple 2D images of the same object viewed at different angles, the desired 3D structure can be fabricated in a single step, greatly reducing printing time.

The 2D light patterns delivered to each plane of the photosensitive resin act accumulatively to produce the desired 3D structure in a single step, greatly reducing printing time. The light doses delivered by each single light exposure are insufficient for crosslinking the photosensitive resin. Accumulation of light doses occurs in specific areas, as defined by the desired 3D geometry, following repeated exposure to the projected 2D light patterns. Photopolymerization subsequently occurs in localized areas where the cumulative adsorbed light dose exceeds the crosslinking threshold.

This threshold behavior arises due to oxygen inhibition of the free radical polymerization process. Resins prepared in and exposed to ambient environment naturally contain molecular oxygen, which is known to act as a scavenger of free radicals. As the rate of free radical scavenging by molecular oxygen is 3-4 order of magnitudes faster that of polymer chain propagation, molecular oxygen in any localized area of the resin must first be sufficiently depleted by reacting with photolyzed photoinitiator radicals before photopolymerization may compete and proceed [44]. Therefore, a minimum light energy dose must first be delivered and absorbed before photopolymerization may occur, representing a threshold that limits the polymerization reaction to localized areas defined by the desired 3D geometry.

Given its unique merits, volumetric 3D printing appears to be well-suited for supporting the envisaged model of timely production of tailored medicines. In this study, for the first time, volumetric 3D printing was employed for the rapid fabrication of 3D-printed tablets (Printlets™). We evaluated the suitability of this technology for pharmaceutical 3DP by printing paracetamol-loaded Printlets based on six different formulations. The morphology, physicochemical properties, and dissolution behavior of these Printlets were investigated. Above all, this work introduces a new technology into the growing armamentarium of 3DP technologies suitable for pharmaceutical 3DP.

2. Material and methods

2.1 Materials

Paracetamol (MW 151.16 g/mol), poly(ethylene glycol) diacrylate (PEGDA 575, average MW 575), poly(ethylene glycol) diacrylate (PEGDA 700, average MW 700), poly(ethylene glycol) (PEG 300, average MW 300), lithium phenyl-2,4,6-trimethylbenzoylphosphinate (LAP, MW 294.21 g/mol, ≥ 95%,), and acetonitrile (ACN, ≥ 99.9%, HPLC grade), were purchased from Sigma-Aldrich (Dorset, UK). Trisodium orthophosphate was purchased from Honeywell Fluka (Buchs, Switzerland). All materials were used as received.

2.2. Preparation of photopolymer solution

Six formulations were prepared and tested for volumetric printing (Table 1). LAP was selected as the photoinitiator due to its maximum absorption wavelength at ~385 nm and paracetamol was selected as the model drug. PEGDA 575 and PEGDA 700 were selected as the photocurable cross-linking acrylate monomers, due to their well-established photoreactivity and crosslinking capabilities [32, 47]. Water and PEG 300 were included as diluents to facilitate drug release. For all formulations, 40 g of resin was prepared comprising 5% (w/w) paracetamol, 0.025% (w/w) LAP, and varying ratios of PEGDA 575:Water or PEGDA 700:PEG 300 (namely 90:10, 65:35, 35:65 (w/w)) in amber vials. The final solution was thoroughly mixed at room temperature until the drug and photoinitiator were completely dissolved (up to 8 hours).

Table 1. Compositions of the tested formulations in volumetric printing.

Formulation	LAP (% w/w)	PEGDA 575 (% w/w)	Water (% w/w)	PEGDA 700 (% w/w)	PEG 300 (% w/w)	Paracetamol (% w/w)	Exposure time (s)
PW90-10	0.025	85.478	9.497	-	-	5	12
PW65-35	0.025	61.734	33.241	-	-	5	7.5
PW35-65	0.025	33.241	61.734	-	-	5	7
PP90-10	0.025	-	-	85.478	9.497	5	16
PP65-35	0.025	-	-	61.734	33.241	5	16.5
PP35-65	0.025	-	-	33.241	61.734	5	16

2.3. Design and principles of volumetric printer

The volumetric printer (FabRx Ltd., UK) is based on a digital light projector (Wintech DLP6500, USA), composed of a Digital mirror device (DMD), a UV light source (385nm), UV optical lenses (f = 210 mm lens) (Figure 1). The DMD panel creates light patterns at high resolution (1050 × 920) and speed. The digital state of each micromirror in the DMD panel can be controlled as being either 0 (dark) or 1 (light-reflecting for photopolymerization) while the photosensitive resin is introduced to the focal plane of the projected image, leading to its crosslinking. The lateral resolution is theoretically limited by the physical size of DMD mirrors, which is 7.6 µm for the selected model; however, experimental printing resolution (i.e., smallest feature size) was determined to be of the order of 10 µm. The images generated in the DMD were projected through a lens into a 50 x 50 mm squared glass cuvette containing the photosensitive resin. 7 UV reflecting mirrors were arranged in different positions in front of the projector to divide the projected image in three parts (Figure 1B-D). This mirror system allows each section of the image (left side projection, right side projection and bottom projection) to be projected onto the corresponding plane of the cuvette. The superposition of these projections occurs in the middle of the cuvette, 21 cm away from the light source (Figure 1B).

For all locations of the 3D geometry to reach the required accumulated light dose and be cured simultaneously, transverse intensity profile gradients were applied to the light beams so that each beam compensates the other. For this, a 3D light absorption and attenuation model was taken into account, governed by the Beer-Lambert equation [$A = \varepsilon cl$], which consider the relationship between the absorbance (A) and the concentration (c), molar absorption coefficient (ε) and optical coefficient (l) of a solution. Absorption is a non-linear phenomenon,

and beyond a certain point, spatial non-uniformity of absorbed energy cannot be adequately compensated for by linear superposition of intensity profiles.

This can be compensated by the inclusion of absorption inhibitor species [48], such as molecular oxygen (O2) dissolved in the biomaterial [44]. However, due to the low shape complexity of the generated structures, it was deemed in this study unnecessary to include absorption inhibitor species to maintain the non-linearity necessary for threshold behavior in the photopolymerization process. The volumetric 3D printing system has been designed to generate 3D structures taking into account the lateral intensity profile of each beam to be able to compensate for axial resolution and to compensate for resin absorption (Figure 2).

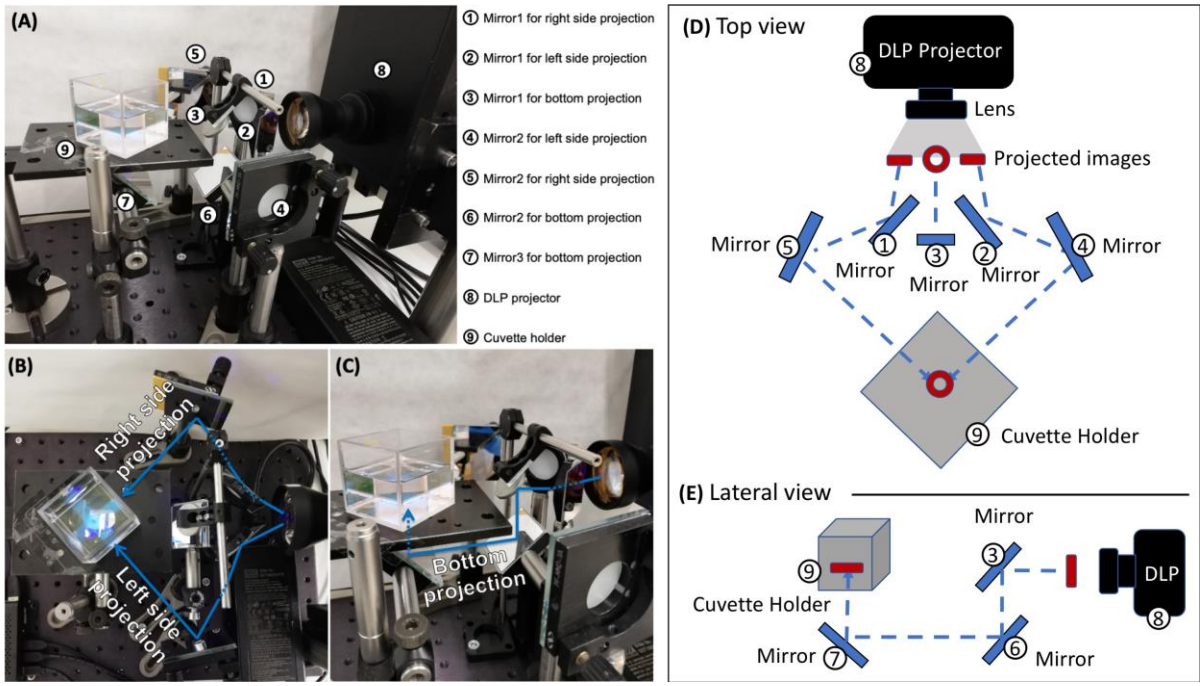

Figure 1. Images of (A) volumetric printer system (legends 1-9 included on the left), (B) top view of the volumetric printer with blue arrows illustrating the path of left and right side projections for irradiating the photosensitive resin along the lateral sides of the cuvette, (C) side view of the volumetric printer with blue arrows illustrating the path of bottom projection for irradiating the photosensitive resin along the underside of the cuvette, and schematic of (D) top and (E) lateral view of the volumetric printer system.

2.4 3D printing process

The selected 3D geometry was a torus, 11 mm diameter x 4 mm height, with a central 3 mm diameter hole. The object was created with 123D Design (Autodesk Inc., USA) and exported

as a stereolithography file (.stl) and uploaded onto an in-house software developed by FabRx (London, UK). The software generated 3 projections (left side projection, right side projection, and bottom projection) based on the uploaded 3D geometry. The software compensates for the superposition of light beams to ensure delivery of equal light doses in all parts of the structure/geometry. The exposure time and light intensity was adjusted within the software according to the photosensitive resin used, as reported in Section 2.2. The final file was subsequently uploaded onto the printer and the optical fields were projected accordingly (Figure 2).

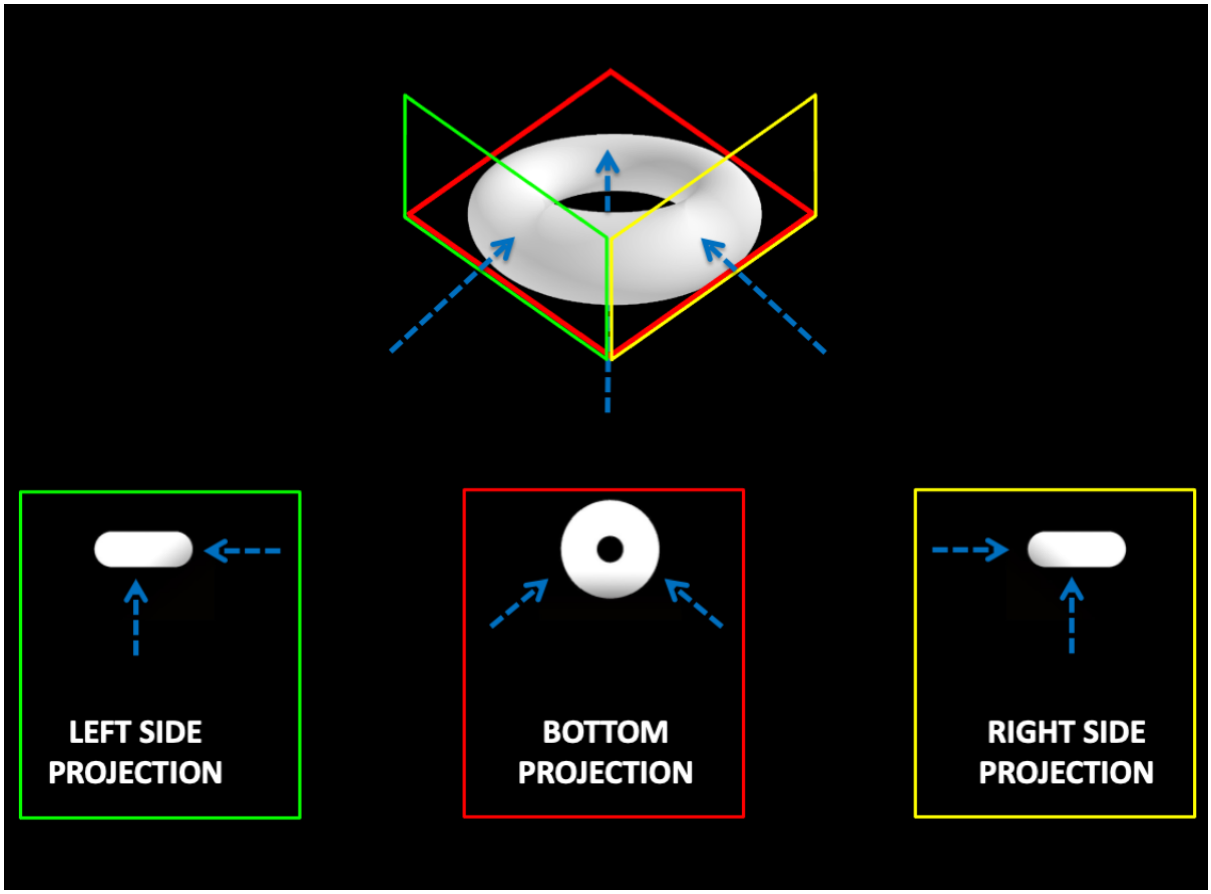

Figure 2. Schematic illustrating the irradiance of the photosensitive resin with three orthogonal light beams (left side projection, right side projection, and bottom projection). Blue dotted arrows represent the light projection.

Photosensitive resin (as prepared in Section 2.2) was loaded into the cuvette and placed onto the cuvette holder of the volumetric printer. Eight Printlets were printed consecutively for each formulation at room temperature. After printing, the Printlets were subjected to post-curing processes akin to that in conventional vat photopolymerization 3DP. Specifically, the Printlets

were gently removed, washed with isopropanol for 10 s, and then placed in an oven (Heraeus I42, Germany) and exposed to UV light (375 nm) using a UV lamp (Philips BLB F8 T5, Netherlands) at 20°C for 1 h.

2.5 Drug photostability study

A stability study was conducted to analyze the possibility of drug degradation in the resin solutions under light exposure at 385 nm and during post-curing. Solutions of paracetamol (5% w/w) in PEGDA 575 and in PEGDA 700 were prepared and placed in the volumetric printer cuvette. The whole cuvette was exposed to light using the same printing conditions (brightness and exposure time) as that during the fabrication of Printlets. Samples (1 mL) were withdrawn at 0 s (control), after 1 cycle of light exposure (20 s), and after 5 cycles of light exposure (5 x 20 s). The cuvette was then subjected to post-curing (exposed to 375 nm light at 20 ºC for 1 h) as described in Section 2.4, and samples (1 mL) were subsequently withdrawn. The concentration of paracetamol in these samples was analyzed using HPLC (Section 2.6.6). The data were analyzed by paired t-test with a 99% confidence interval ($p < 0.01$) to determine statistically significant differences between the paracetamol concentrations in the test and control samples.

2.6 Characterization of the resins and the Printlets

2.6.1 Environmental scanning electron microscopy (ESEM)

Printlets were cut in half and attached onto a self-adhesive carbon disc mounted on a 25 mm aluminum stub, which was coated with 25 nm of gold using a sputter coater. The stub was then placed into a FEI Quanta 200 FEG Scanning Electron Microscope (FEI, UK) at 5 kV accelerating voltage using secondary electron detection to obtain the cross-section images of the Printlets.

2.6.2 Thermal Analysis

Differential scanning calorimetry (DSC) was used to characterize the thermal behavior of the 3D printed formulations. DSC measurements were carried out, in duplicate, using a DSC Q200 (TA Instruments, New Castle, DE, USA) with a refrigerated cooling accessory (RCS), at a

heating rate of 10°C/min. The calorimeter was calibrated for baseline using no pans, for cell constant and temperature using indium (melting point 156.61°C, enthalpy of fusion 28.71 J/g), and for heat capacity using sapphire standards. The range of the temperature was 0-200°C and nitrogen was used as the purge gas at a flow rate of 50 mL/min for all the experiments. All experiments were performed using non-hermetic aluminum pans, in which 3–5 mg of blends were accurately weighed, and then covered with the lid. Data were collected with TA Advantage software for Q series (version 2.8.394) and analyzed using TA Instruments Universal Analysis 2000. All melting temperatures are reported as extrapolated peak unless otherwise stated.

2.6.3 X-ray powder diffraction (XRPD)

X-ray powder diffraction patterns were obtained in a D8 Advance (Bruker, Billerica, MA, USA) using the Bragg-Brentano focusing geometry, equipped with a sealed X-ray tube ((CuKα1 (λ = 1.5406 Å)) and a LYNXEYE-type detector. The intensity and voltage applied were operating at 40 mA and 40 kV, respectively. The diffractograms were obtained in the 2θ angular range of 3-60º with a step of 0.02º and a counting time of 2 s per step. Samples were deposited on an oriented Si(511) plate to avoid scattering noise caused by a glass support. Samples were rotated during measurement to obtain optimal peak profiles for analysis and to minimize the effect of the preferential orientation. Mathematical analysis of the obtained diffractograms was performed using the HighScore Plus (version 3.0d) software.

2.6.4 X-ray micro computed tomography (micro-CT)

To visualize the internal structure of the Printlets, a high-resolution X-ray micro computed tomography (Micro-CT) scanner (SkyScan1172, Bruker-microCT, Kontich, Belgium) was used as in a previous study [33]. Each image was obtained by rotating the Printlet through 180° with a frame averaging of 4 and a 0.5° rotation step using medium camera resolution (2000 × 1048 pixels). Image reconstruction was performed using NRecon software (Version 1.7.0.4, Bruker-microCT, Kontich, Belgium) and the reconstructed images were processed and visualized using the Ctan software (version 1.15.4).

2.6.5. Fourier-Transform infrared spectroscopy (FTIR)

The infrared spectra of paracetamol, pre-cured photosensitive resins, and Printlet were collected using a Spectrum 100 FTIR spectrometer (PerkinElmer, Waltham, MA). All samples were scanned between 4000 and 650 cm^{-1} at a resolution of 1 cm^{-1} resolution for 6 scans.

2.6.6. Drug content in the photopolymer solution and Printlets

Paracetamol-loaded Printlets prepared using the volumetric printer were crushed into fine particles using a mortar and a pestle, placed in a volumetric flask with acetonitrile (25 mL), and subjected to magnetic stirring overnight. Samples of solution were filtered through 0.22 µm filters (Millipore Ltd., Ireland) and the concentration of drug was determined using HPLC (JASCO LC-4000 Series, Jasco, Spain). The validated HPLC assay entailed injecting 20 µL of sample into a Waters Spherisorb 5 µm C8 column, 4.6 mm x 250 mm (Waters, Milford, MA, USA). The compounds were separated using a mobile phase composed of water (85% v/v) and methanol (15% v/v), which was pumped at a flow rate of 1 mL/min. The temperature was maintained at 40 °C and the eluents were assessed at a wavelength of 247 nm. The retention time was 8 min. All measurements were made in duplicate.

2.6.7 In vitro dissolution studies

The drug release profiles of the Printlets were evaluated using a SR8-Plus Dissolution Test Station (Hanson Research, Chatsworth, CA, USA) with USP-II apparatus. The Dissolution Test Station was connected to a pump system Auto Plus DissoScan (Hanson Research, Chatsworth, CA, USA). The speed of the paddles was set at 50 rpm with a temperature of 37 ± 0.5 °C. The Printlets were dropped in 750 mL of 0.1 M HCl for 2 h to simulate gastric conditions. After 2 h, 250 mL of trisodium phosphate solution (0.2 M) was added into each vessel and the pH was adjusted to 6.8 using 1 M NaOH or 1 M HCl solutions to simulate intestinal conditions. During the dissolution assay, samples were automatically withdrawn and filtered through 10 µm filters. The concentration of paracetamol in each sample solution was determined using an in-line UV spectrophotometer (Agilent 8453, Germany) at a wavelength of 243 nm. At the end of the assay, 1 mL of sample was withdrawn from each vessel, filtered through 0.22 µm filters (Millipore Ltd., Ireland), and analyzed using HPLC to determine the final amount of drug released. Tests were conducted in triplicate under sink conditions. Data were reported throughout as mean ± standard deviation (n=3).

3. Results and discussions

A volumetric 3D printer was adapted and used for the first time to rapidly fabricate drug-loaded Printlets with promising results. Drug-free Printlets were initially printed successfully to obtain an approximate on the required exposure time (data not reported). Paracetamol readily dissolved in the photosensitive resin formulations. A torus shape was selected as it affords a greater surface area to volume ratio compared to a disc and therefore conceivably accelerates the rate of drug release [49]. Additionally, in a previous study investigating patient acceptability of 3D printed medicines, it was found that torus Printlets achieved the highest acceptability score [50]. All paracetamol-loaded Printlets were successfully fabricated by volumetric 3D printing (Figure 3).

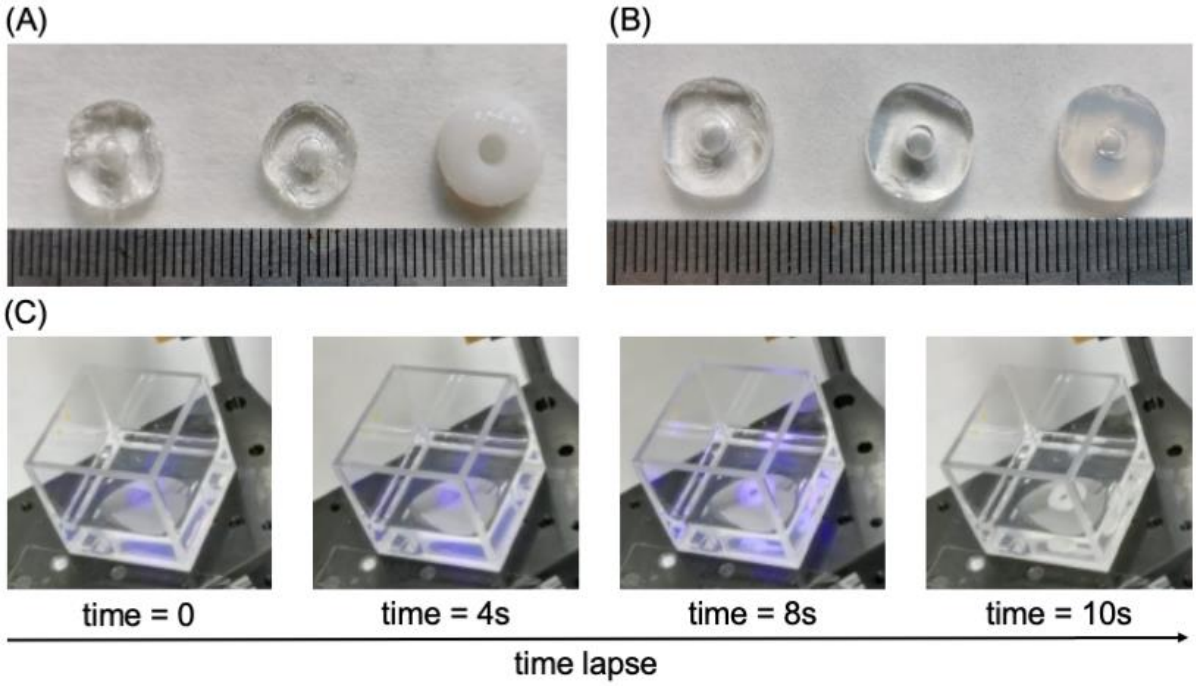

Figure 3. Photographs of the Printlets, A) PW90-10, PW65-35, PW35-65; B) PP90-10, PP65-35, PP35-65, and C) sequential view of the cuvette during the Printlet fabrication process. Scale in cm.

Multiple iterations of printing parameters were evaluated before finally establishing an optimal light intensity equivalent to 67% of the projector's projection brightness. The cumulative light dose required to achieve satisfactory degree of cross-linking varied for each formulation since they were each composed of different concentrations of photopolymerizable acrylate monomers and diluents. Accordingly, exposure times were adjusted for each formulation, as

expressed in Table 1. Printlets and photosensitive resins containing lower concentrations of PEGDA were opaquer (Figure 3). This is due to microphase separation occurring between solutions of relatively hydrophobic PEGDA and aqueous solutions of PEG and water [51]. With increasing proportion of hydrophilic components (water or PEG) in the photosensitive resin, a greater degree of phase separation occurs to give a thicker emulsion appearance. All Printlets, regardless of their composition, were largely uniform in physical dimensions (Table 2).

Table 2. Results of the dimensions and drug loading for the Printlets (*n* = 8)

Printlet	Diameter (mm)	Thickness (mm)	Drug loading in Printlets (%)	Drug content in photosensitive resin (%)
PW90-10	10.83 ± 0.29	4.16 ± 0.29	4.39 ± 0.41	5.04 ± 0.01
PW65-35	11.17 ± 0.29	4.33 ± 0.29	4.48 ± 0.31	4.95 ± 0.03
PW35-65	11.67 ± 0.58	4.17 ± 0.29	4.54 ± 0.35	5.05 ± 0.03
PP90-10	11.17 ± 0.29	4.17 ± 0.29	4.65 ± 0.23	5.02 ± 0.01
PP65-35	11.67 ± 0.58	3.67 ± 0.29	4.43 ± 0.36	4.99 ± 0.04
PP35-65	11.17 ± 0.29	4.17 ± 0.29	4.44 ± 0.37	4.99 ± 0.01

The observed drug loading of the fabricated Printlets was slightly lower than the theoretical drug content (5 wt%) (Table 2). Previous studies on the fabrication of paracetamol-loaded Printlets have indicated the photostability of paracetamol upon visible light irradiance [52]. However, the stability of paracetamol during 3DP using 385 nm light has not been investigated. Therefore, photostability studies were carried out to investigate if the underlying reason for the lower drug loading was due to photodegradation of paracetamol at 385 nm. The results indicated that there was no statistically significant loss of paracetamol ($p < 0.01$) upon exposure to light at a wavelength of 385 nm and of the same intensity as the one used in the volumetric 3D printing process, as well as after exposure to post-curing conditions (Figure 4). This corroborates with previous studies demonstrating the effective loading of a range of active pharmaceutical ingredients into photopolymerizable resin without observable degradation upon exposure to UV light, including narrow therapeutic index drugs such as warfarin, theophylline, and docetaxel [17, 53-55].

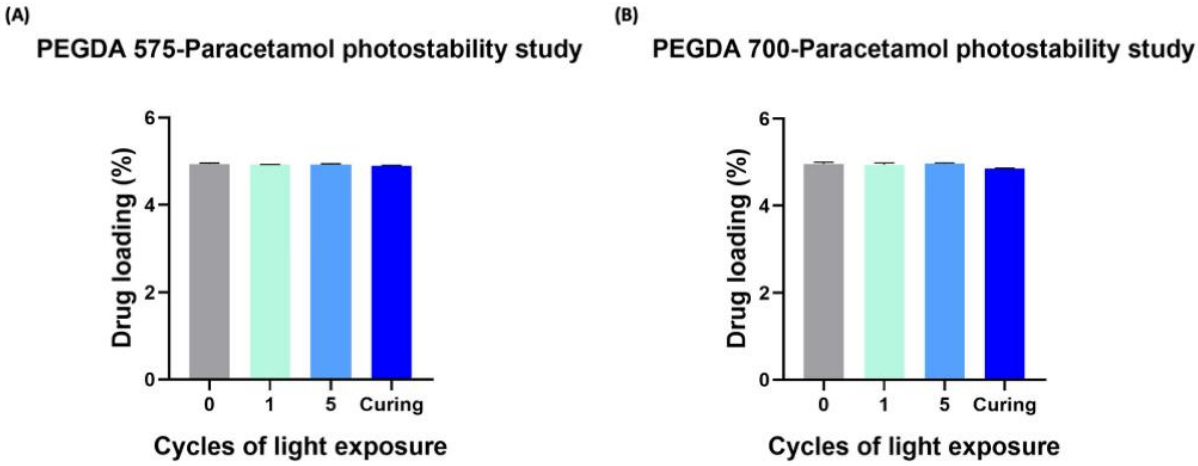

Figure 4. Results of photostability study of paracetamol in (A) PEGDA 575 and (B) PEGDA 700, exposed to 1 and 5 cycles of 385 nm light of the same intensity used in the volumetric 3D printing process, and 1 hours of post-curing under 375 nm light at 20 ºC for 1 hour. All measurements are expressed as mean ± standard deviation (n = 3).

FTIR spectroscopy was used to probe into potential chemical interactions between paracetamol and the photopolymer (PEGDA) in the preparation of Printlets (Figure 5).

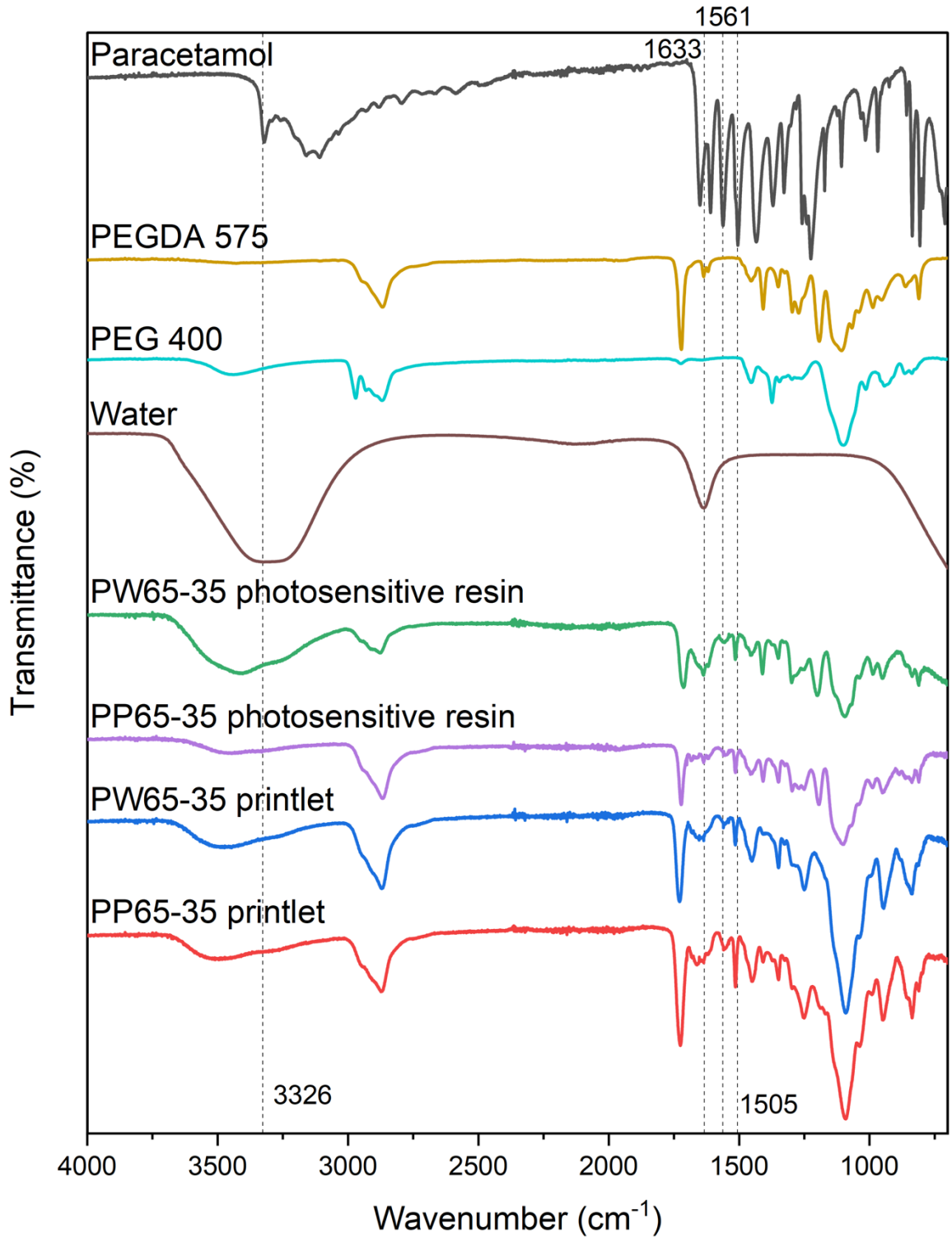

Figure 5. FTIR spectra of paracetamol, PEGDA 575, PEG 400, water and PW65-35 and PP65-35 photosensitive resin and Printlets.

The spectrum of paracetamol powder showed characteristic vibrational peaks at 3326 cm^{-1} (O-H stretching), 1561 cm^{-1} (N-H amide stretching), and 1505 cm^{-1} (C-H stretching) [56, 57].

Apart from the peak at 3326 cm^{-1}, these absorption bands could be clearly observed in the spectra of PW65-35 and PP65-35 photosensitive resins and Printlets, indicating that there were no detectable chemical interactions, such as Michael's addition, between the drug and the photopolymers. The peak at 3326 cm^{-1} was not observable as it was masked by broad peaks at similar wavelengths from water or PEG 400. The spectrum of PEGDA 575 was included as a reference to show its distinctive acrylate peaks at 1722 cm^{-1} (C=O stretching) and 1633 cm^{-1} (C=C stretching). Specifically, the band at 1633 cm^{-1} (C=C stretching) was used to confirm that photopolymerization of PEGDA monomers had occurred, as the conversion of C=C to C-C bonds during photopolymerization will attenuate this vibrational band [58]. Therefore, neither the photodegradation of paracetamol nor chemical interactions with PEGDA account for the observed negative deviation in drug loading. Instead, one possible reason could be an incomplete drug extraction from the polymer matrix [32]. This is turn could be due to an equilibrium being reached between the paracetamol concentration in the extraction medium and that within the polymer matrix at the end of the extraction process, thus preventing any further diffusion of paracetamol out of the polymer matrix.

ESEM imaging was used to visualize the surface and cross sections of the Printlets (Figure 6). The ESEM images of all Printlets revealed smooth surfaces with no apparent layers, confirming the absence of any crystalline drug. The layerless structure of the Printlets were as predicted since the entire 3D object was fabricated simultaneously in volumetric 3D printing as opposed to a layer-by-layer process. It is noted that the ESEM images of all Printlets depict a core-shell structure, which could have arisen because of the post-curing process in the UV curing oven. As the intensity of UV light attenuates as it penetrates through the Printlet, residual uncured PEGDA monomers on the surface of the Printlet would have been exposed to a higher intensity of light compared to those within the core of the Printlet. The ESEM images of PW35-65 and PP35-65 Printlets also appear to be less homogenous compared to other Printlets, further suggesting that a greater extent of microphase separation had occurred with photosensitive resins comprising a relatively higher proportion of hydrophilic components (water or PEG).

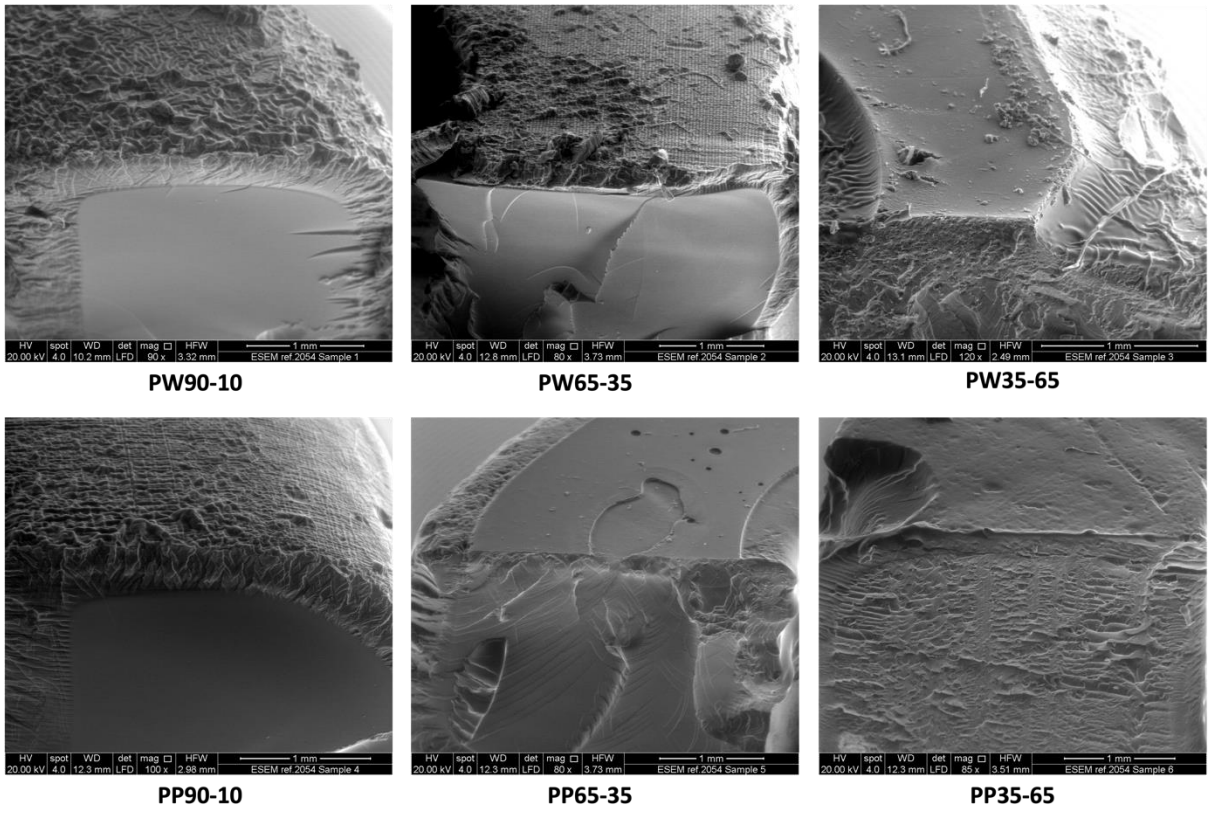

Figure 6. ESEM images of cross sections of different Printlets after all processing steps. The scale bar is equivalent to 1mm.

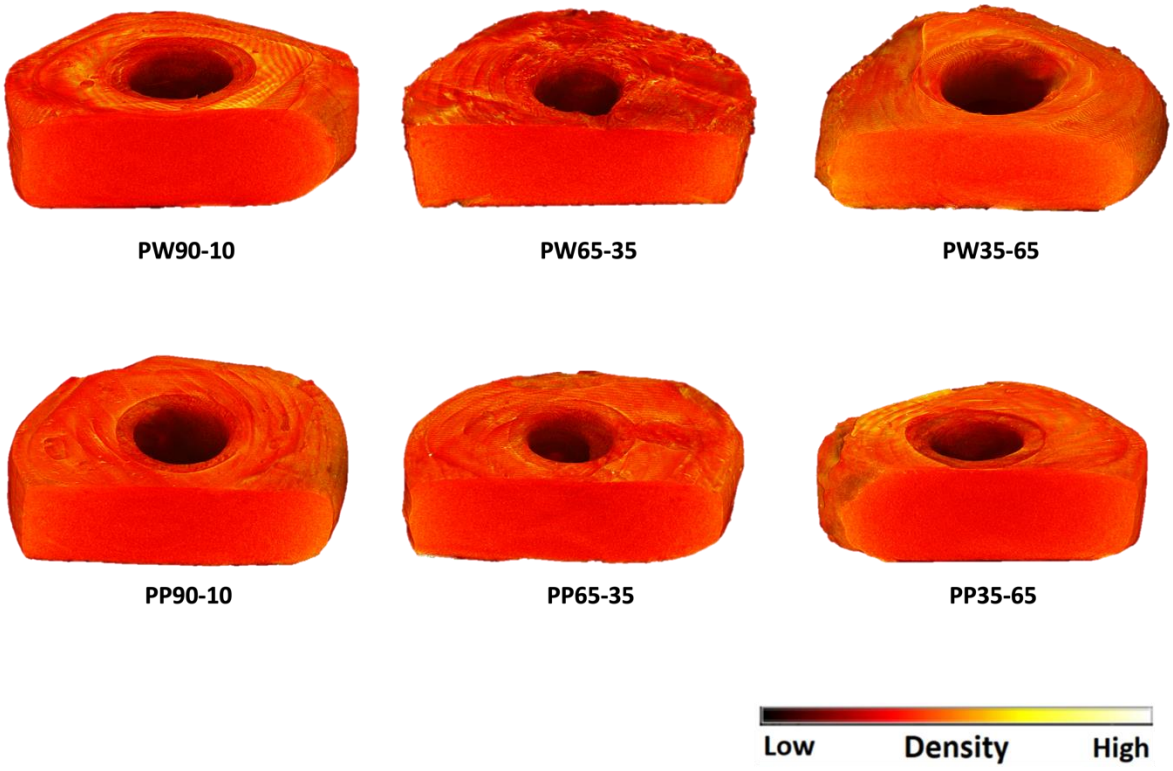

Figure 7. X-ray micro-CT images of different Printlets. The scale bar in the micro-CT image is representative of density.

X-ray micro-CT imaging was used to visualize the internal structure and calculate the density of the Printlets (Figure 7). From investigating each Printlet individually, it can be observed that the entire structure of the Printlet is equally dense, suggesting that no particulate and layering artifacts were present. No discernible density difference could be observed between Printlets derived from different formulations, indicating that the selected exposure times for each formulation was successful in accommodating for varying monomer concentrations and fabricating Printlets of equal densities.

DSC and XRD analysis of the Printlets and paracetamol was performed to determine the physical state of the drug in the Printlets (Figure 8). DSC data showed that paracetamol melts at 169°C. The absence of paracetamol melting peaks in the thermograms of the Printlets indicated that the drug was completely dissolved in the initial PEGDA solutions and remained molecularly dispersed in the solid Printlets (Figure 8A). The broad endotherm peaks at around 100°C observed in the thermograms of the Printlets were attributed to water loss upon heating. This is further supported by the acquired X-ray diffractograms, wherein the crystalline peaks corresponding to paracetamol are absent in the diffractograms of all the Printlets (Figure 8B).

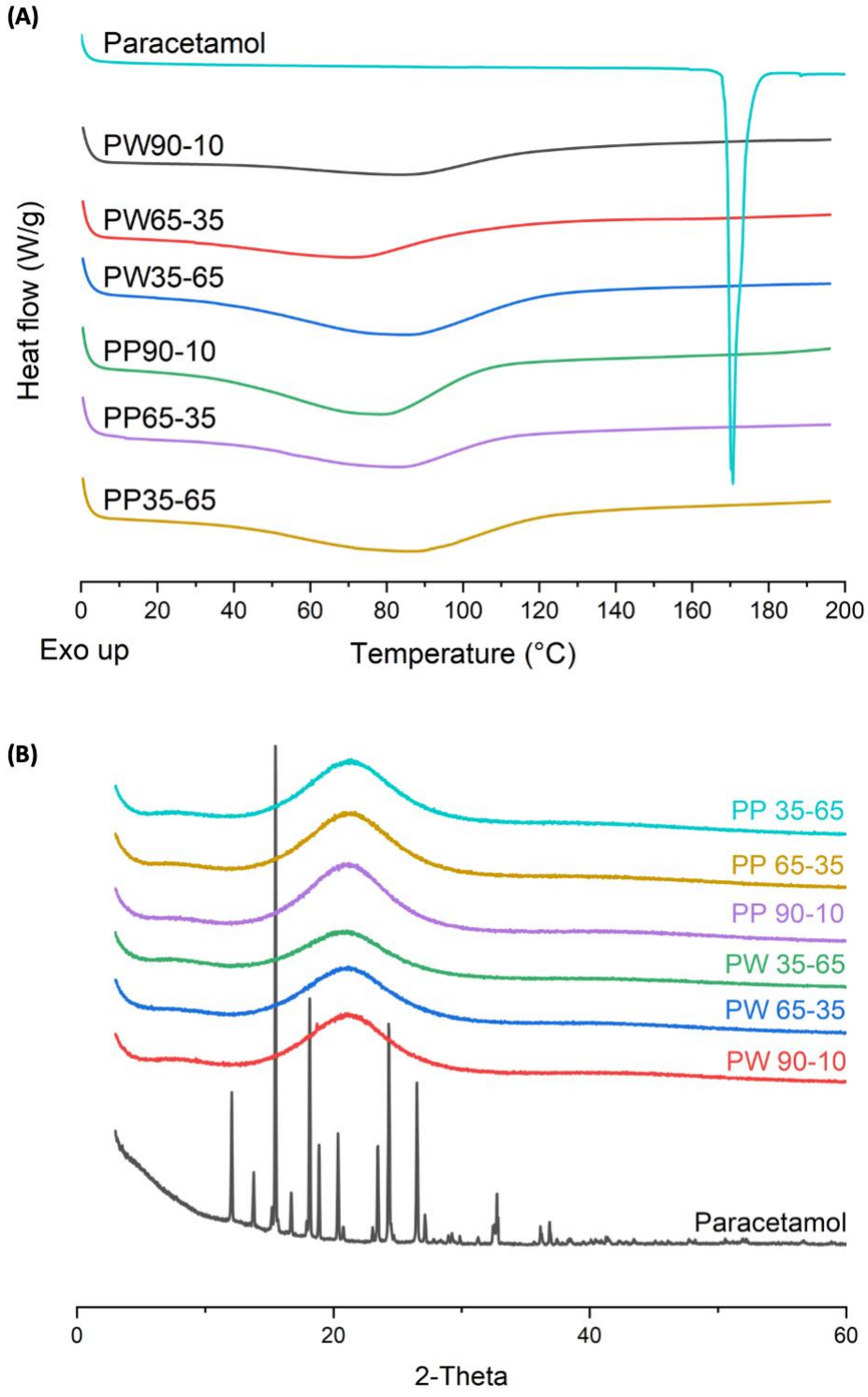

Figure 8. (A) DSC thermograms of pure paracetamol and different Printlets, and (B) X-ray powder diffractograms of pure paracetamol and Printlets.

3.4 In vitro dissolution tests

The dissolution profiles showed that paracetamol release commenced during the gastric phase (pH 1.2) and were not affected by the change of pH in the dissolution media (to pH 6.8) (Figure 9). 90 % of paracetamol was released within 7 hours from PW35-65 Printlets, while it took PW65-35 Printlets 10.5 hours and PW90-10 Printlets 16 hours to achieve the same extent of drug release (Figure 9A). Likewise, between PEGDA 700-PEG300 formulations, 90% of paracetamol was released within 4.5 hours for the PP35-65 Printlets while it took PP65-35 and PP90-10 Printlets 7.5 hours and 14.5 hours to achieve the same extent of drug release, respectively (Figure 9B). There were no observable changes in the Printlets' color and size before and after dissolution, suggesting that drug release occurred via diffusion out of the insoluble polymer matrix. The differences observed in drug release rates can be mainly attributed to the varying density of crosslinked polymer networks, which is in turn influenced by the monomer-to-diluent ratio and the types of monomers and diluent used. In relation to the former, higher percentage of diluents enhances the rate of drug release. This is because diluents, such as water and PEG 300, are not incorporated into the crosslinked photopolymerized polymer matrix. Consequently, their presence results in less dense matrices that facilitates greater molecular mobility and consequently faster drug diffusion out of the Printlet [32].

The type of monomers and diluents used were also observed to influence the rate of drug release. Comparing the dissolution profiles of PEGDA 575–Water and PEGDA 700–PEG300, it is noticeable that PEGDA 575-Water Printlets released paracetamol at a slower rate than PEGDA 700-PEG300 Printlets with the same monomer-to-diluent ratio. This can be attributed to denser crosslinked polymer networks in PEGDA 575-Water Printlets that are in turn due to two underlying causes: (1) the lower molecular weight and hence shorter chain of PEGDA 575 compared to PEGDA 700, and (2) the smaller molecular size of water compared to PEG300. Shorter chain photopolymerizable monomers form denser crosslinked polymer networks due to the shorter molecular distance between two acrylate groups or crosslinking junctions [59]. In a similar way, diluents with smaller molecular size lead to smaller pore sizes within the Printlet when they are subsequently removed. Taken together, it is conceivable that PEGDA 700-PEG300 Printlets possessed less dense crosslinked polymer networks than PEGDA 575-Water Printlets of equivalent monomer-to-diluent ratio, allowing paracetamol to diffuse out of their structure at a faster rate.

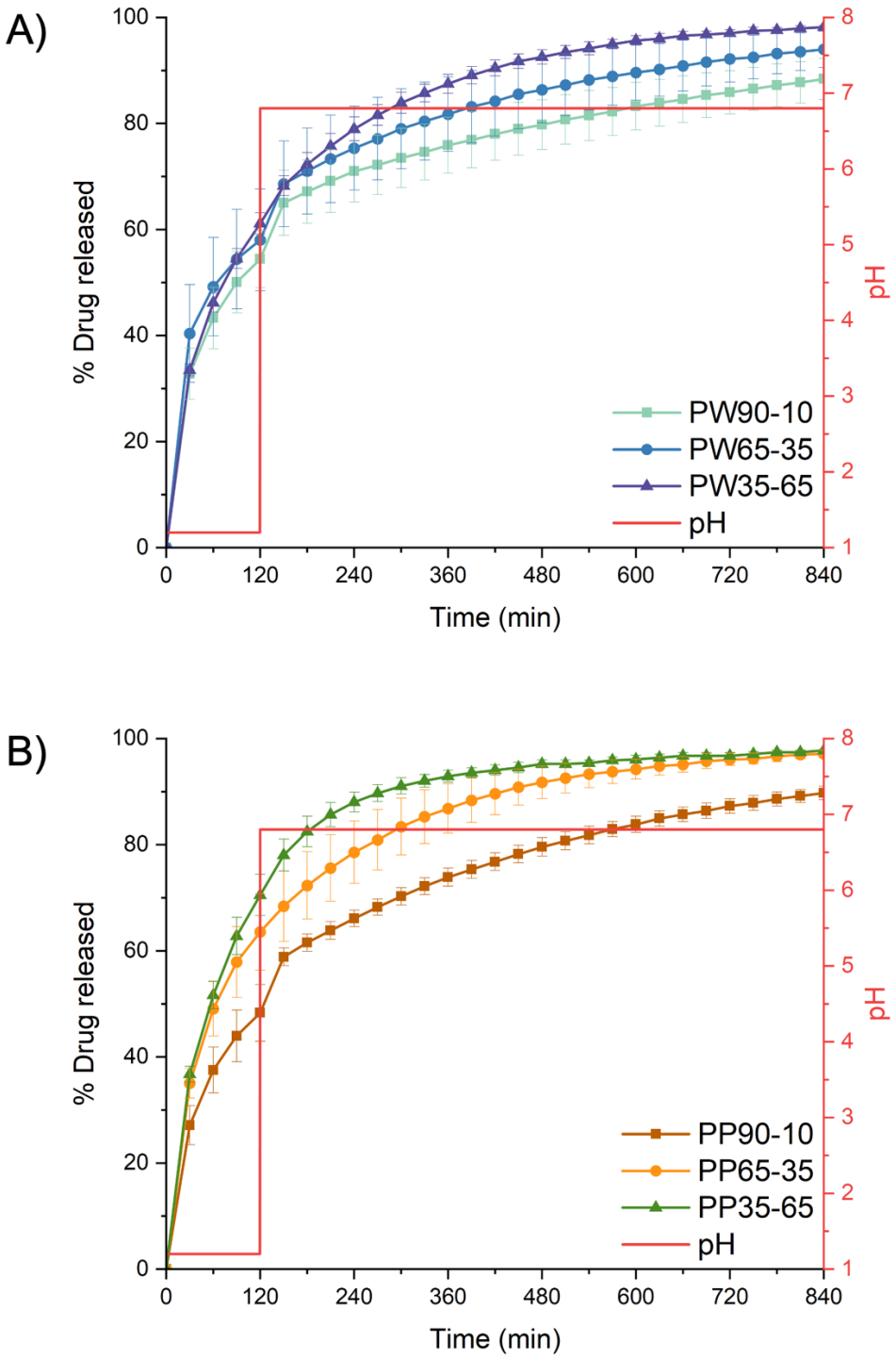

Figure 9. Paracetamol dissolution profiles from (A) PEGDA 575–Water Printlets and (B) PEGDA 700-PEG 300 Printlets. The pH values of the media are indicated with the red line.

Similar PEGDA 700-PEG 300 formulations were used in a previous study investigating the use of SLA for producing paracetamol-loaded Printlets [52]. Strikingly, comparing the dissolution profiles of SLA and volumetric 3DP Printlets derived from similar PEGDA 700-PEG300 formulation revealed that volumetric 3DP Printlets released paracetamol at a faster rate than SLA Printlets. For instance, PEGDA 700 – PEG300 (35%/65% w/w) Printlets

produced by SLA released ~50% of paracetamol in 2 hours, while that produced by volumetric 3DP in this study released ~70% of paracetamol within the same time frame. This could be due to differences in the intensity and wavelength of the light source (405 nm laser in SLA compared to 385 nm projector in volumetric 3DP). Additionally, a different photoinitiator, diphenyl(2,4,6-trimethylbenzoyl) phosphine oxide (DPPO), possessing a different local absorbance maximum and molar extinction coefficient than LAP was used in the previous study. In all, these factors could have resulted in different degrees of excitation of photoinitiator molecules, which in turn affects the degree of acrylate functional group conversion and crosslinking.

The experimental data presented above demonstrates the suitability of this novel technology for fabricating high quality and consistent personalized medicines within seconds. To realize the deployment of this technology, it will be necessary to investigate the effect of numerous parameters and develop a system to automatically optimize them for different photosensitive resins. These include, but are not limited to, the light intensity, molar extinction coefficient of photoinitiators at the relevant wavelength of light, the type of crosslinkable monomers and diluents used, the active pharmaceutical ingredient, and the geometry of the desired object. By consolidating these data, artificial intelligence (AI) could then be employed to accelerate the development process, as exemplified by its use to predict the 3D printing performance of Printlets prepared by other 3DP technologies [60-62]. Advances in the optimization of printing parameters could then see the fabrication of more complex geometries to extend the application of volumetric 3DP to drug-loaded medical devices. Volumetric 3D printing can also be integrated with non-invasive diagnostics or drug monitoring strategies, notably in the form of biosensors, to provide a dynamic system of tailoring medicines in response to these clinical outputs [63, 64]. The combination of volumetric 3DP with these emerging technologies could enable a virtuous cycle of personalized medicine and provide significant improvements in health outcomes [1].

It is pertinent to acknowledge that further research will be needed to investigate the biocompatibility of the photosensitive resins used. This might entail a systemic evaluation of the cytocompatibility and toxicology profile of individual components of the formulation to identify potential cytotoxic species that would need replacement, as well as that of products derived from the photopolymerization reaction. Ongoing research in 3D bioprinting offers optimism over the cytocompatibility of the materials used. PEGDA is a commonly used photopolymerizable monomer in bioprinting of 3D cell cultures and tissue models [65-68], and LAP is also being employed as a photoinitiator in bioprinting formulations [69]. Therefore, the development of volumetric 3D printing as a viable technology for personalized pharmaceutical

manufacturing can be accelerated by continued efforts in optimizing relevant parameters and extracting learnings from similar fields.

5. Conclusions

Volumetric 3D printing was successfully employed, for the first time, to prepare Printlets containing paracetamol. Paracetamol-loaded torus Printlets were successfully fabricated within 7 to 17 seconds, representing the fastest way of producing personalized Printlets via 3DP thus far. Drug release profiles could be tuned by varying the ratio of photopolymerizable monomers to diluents in the formulation. The data presented in this study confirms the suitability of this novel technology for printing medicines at rapid speeds, making it ideal for decentralized pharmaceutical manufacturing. Demand for a technology that affords versatile and fast production of medicinal products will continue to grow with increasing recognition that a tailored approach towards patient care is superior to the traditional one-size-fits-all model. Therefore, with further research and optimization, we foresee volumetric 3DP becoming a powerful tool in the virtuous cycle of personalized medicines.

Acknowledgments:

This work was supported by the Xunta de Galicia (Consellería de Culture, Educación e Universidade) [grant number ED481A, 2020/21].

References

1. Seoane-Viaño, I., et al., *Translating 3D printed pharmaceuticals: From hype to real-world clinical applications.* Advanced Drug Delivery Reviews, 2021. **174**: p. 553-575.

2. Capel, A.J., et al., *3D printing for chemical, pharmaceutical and biological applications.* Nature Reviews Chemistry, 2018. **2**(12): p. 422-436.

3. Xu, X., et al., *A customizable 3D printed device for enzymatic removal of drugs in water.* Water Research, 2022. **208**: p. 117861.

4. Choong, Y.Y.C., et al., *The global rise of 3D printing during the COVID-19 pandemic.* Nature Reviews Materials, 2020. **5**(9): p. 637-639.

5. Prabhakar, P., et al., *3D-Printed Microfluidics and Potential Biomedical Applications.* Frontiers in Nanotechnology, 2021. **3**(6).

6. Medicines & Healthcare products Regulatory Agency. *Consultation on Point of Care manufacturing*. 2021 12 August 2021 [cited 2021 10 September]; Available from: https://www.gov.uk/government/consultations/point-of-care-consultation/consultation-on-point-of-care-manufacturing.

7. Trenfield, S.J., et al., *Advancing pharmacy and healthcare with virtual digital technologies.* Advanced Drug Delivery Reviews, 2022. **182**: p. 114098.

8. Awad, A., et al., *Connected healthcare: Improving patient care using digital health technologies.* Advanced Drug Delivery Reviews, 2021. **178**: p. 113958.

9. Durga Prasad Reddy, R. and V. Sharma, *Additive manufacturing in drug delivery applications: A review.* International Journal of Pharmaceutics, 2020. **589**: p. 119820.

10. Evans, S.E., et al., *2D and 3D inkjet printing of biopharmaceuticals – A review of trends and future perspectives in research and manufacturing.* International Journal of Pharmaceutics, 2021. **599**: p. 120443.

11. Melocchi, A., et al., *Shape memory materials and 4D printing in pharmaceutics.* Advanced Drug Delivery Reviews, 2021. **173**: p. 216-237.

12. Borandeh, S., et al., *Polymeric drug delivery systems by additive manufacturing.* Advanced Drug Delivery Reviews, 2021. **173**: p. 349-373.

13. Tan, Y.J.N., et al., *Customizable drug tablets with constant release profiles via 3D printing technology.* International Journal of Pharmaceutics, 2021. **598**: p. 120370.

14. Zheng, Y., et al., *Melt extrusion deposition (MED™) 3D printing technology – A paradigm shift in design and development of modified release drug products.* International Journal of Pharmaceutics, 2021. **602**: p. 120639.

15. Kuźmińska, M., et al., *Solvent-free temperature-facilitated direct extrusion 3D printing for pharmaceuticals.* International Journal of Pharmaceutics, 2021. **598**: p. 120305.

16. Eleftheriadis, G.K., et al., *Modular design principle based on compartmental drug delivery systems.* Advanced Drug Delivery Reviews, 2021. **178**: p. 113921.

17. Xu, X., et al., *Smartphone-enabled 3D printing of medicines.* International Journal of Pharmaceutics, 2021. **609**: p. 121199.

18. Robles-Martinez, P., et al., *3D printing of a multi-layered polypill containing six drugs using a novel stereolithographic method.* Pharmaceutics, 2019. **11**(6).

19. Xu, X., et al., *Stereolithography (SLA) 3D printing of an antihypertensive polyprintlet: Case study of an unexpected photopolymer-drug reaction.* Additive Manufacturing, 2020. **33**: p. 101071.

20. Pereira, B.C., et al., *Additive manufacturing of a Point‐of‐Care "Polypill:" Fabrication of concept capsules of complex geometry with bespoke release against cardiovascular disease.* Advanced Healthcare Materials, 2020. **9**(13): p. 2000236.

21. Awad, A., et al., *3D Printed Tablets (Printlets) with Braille and Moon Patterns for Visually Impaired Patients.* Pharmaceutics, 2020. **12**(2): p. 172.

22. Tiboni, M., et al., *3D printed clotrimazole intravaginal ring for the treatment of recurrent vaginal candidiasis.* International Journal of Pharmaceutics, 2021. **596**: p. 120290.

23. Janusziewicz, R., et al., *Design and Characterization of a Novel Series of Geometrically Complex Intravaginal Rings with Digital Light Synthesis.* Advanced Materials Technologies, 2020. **5**(8): p. 2000261.

24. Vivero-Lopez, M., et al., *Anti-biofilm multi drug-loaded 3D printed hearing aids.* Materials Science and Engineering: C, 2021. **119**: p. 111606.

25. Holländer, J., et al., *Three-dimensional printed PCL-based implantable prototypes of medical devices for controlled drug delivery.* Journal of pharmaceutical sciences, 2016. **105**(9): p. 2665-2676.

26. Martin, N.K., et al., *Fused deposition modelling for the development of drug loaded cardiovascular prosthesis.* International Journal of Pharmaceutics, 2021. **595**: p. 120243.

27. International, A., *Standard Guidelines for Design for Additive Manufacturing*. 2016.

28. Elbadawi, M., et al., *Harnessing artificial intelligence for the next generation of 3D printed medicines.* Advanced Drug Delivery Reviews, 2021. **175**: p. 113805.

29. Xu, X., et al., *Vat photopolymerization 3D printing for advanced drug delivery and medical device applications.* Journal of Controlled Release, 2021. **329**: p. 743-757.

30. Li, W., et al., *Recent Advances in Formulating and Processing Biomaterial Inks for Vat Polymerization‐Based 3D Printing.* Advanced Healthcare Materials, 2020. **9**(15): p. 2000156.

31. Ng, W.L., et al., *Vat polymerization-based bioprinting—process, materials, applications and regulatory challenges.* Biofabrication, 2020. **12**(2): p. 022001.

32. Wang, J., et al., *Stereolithographic (SLA) 3D printing of oral modified-release dosage forms.* Int J Pharm, 2016. **503**(1-2): p. 207-12.

33. Xu, X., et al., *Stereolithography (SLA) 3D printing of a bladder device for intravesical drug delivery.* Materials Science and Engineering: C, 2021. **120**: p. 111773.

34. Kadry, H., et al., *Digital light processing (DLP)3D-printing technology and photoreactive polymers in fabrication of modified-release tablets.* European Journal of Pharmaceutical Sciences, 2019. **135**: p. 60-67.

35. Lim, S.H., et al., *High resolution photopolymer for 3D printing of personalised microneedle for transdermal delivery of anti-wrinkle small peptide.* Journal of Controlled Release, 2021. **329**: p. 907-918.

36. Krkobabić, M., et al., *Digital light processing (DLP) 3D printing of atomoxetine hydrochloride tablets using photoreactive suspensions.* Pharmaceutics, 2020. **12**(9): p. 833.

37. Karakurt, I., et al., *Stereolithography (SLA) 3D Printing of Ascorbic Acid Loaded Hydrogels: A Controlled Release Study.* International Journal of Pharmaceutics, 2020: p. 119428.

38. Xu, X., et al., *3D Printed Punctal Plugs for Controlled Ocular Drug Delivery.* Pharmaceutics, 2021. **13**(9): p. 1421.

39. Uddin, M.J., et al., *3D printed microneedles for anticancer therapy of skin tumours.* Materials Science and Engineering: C, 2020. **107**: p. 110248.

40. Vaut, L., et al., *3D printing of reservoir devices for Oral drug delivery: from concept to functionality through design improvement for enhanced Mucoadhesion.* ACS Biomaterials Science & Engineering, 2020. **6**(4): p. 2478-2486.

41. Paunović, N., et al., *Digital light 3D printing of customized bioresorbable airway stents with elastomeric properties.* Science Advances, 2021. **7**(6): p. eabe9499.

42. Tumbleston John, R., et al., *Continuous liquid interface production of 3D objects.* Science, 2015. **347**(6228): p. 1349-1352.

43. Janusziewicz, R., et al., *Layerless fabrication with continuous liquid interface production.* Proceedings of the National Academy of Sciences, 2016. **113**(42): p. 11703.

44. Shusteff, M., et al., *One-step volumetric additive manufacturing of complex polymer structures.* Science advances, 2017. **3**(12): p. eaao5496.

45. Kelly, B.E., et al., *Volumetric additive manufacturing via tomographic reconstruction.* Science, 2019. **363**(6431): p. 1075-1079.

46. Loterie, D., P. Delrot, and C. Moser, *High-resolution tomographic volumetric additive manufacturing.* Nature communications, 2020. **11**(1): p. 1-6.

47. Miri, A.K., et al., *Microfluidics-Enabled Multimaterial Maskless Stereolithographic Bioprinting.* Adv Mater, 2018. **30**(27): p. e1800242.

48. de Beer Martin, P., et al., *Rapid, continuous additive manufacturing by volumetric polymerization inhibition patterning.* Science Advances, 2019. **5**(1): p. eaau8723.

49. Goyanes, A., et al., *Effect of geometry on drug release from 3D printed tablets.* International Journal of Pharmaceutics, 2015. **494**(2): p. 657-663.

50. Goyanes, A., et al., *Patient acceptability of 3D printed medicines.* International Journal of Pharmaceutics, 2017. **530**(1): p. 71-78.

51. Stenekes, R.J.H., et al., *The use of aqueous PEG/dextran phase separation for the preparation of dextran microspheres.* International Journal of Pharmaceutics, 1999. **183**(1): p. 29-32.

52. Wang, J., et al., *Stereolithographic (SLA) 3D printing of oral modified-release dosage forms.* International Journal of Pharmaceutics, 2016. **503**(1): p. 207-212.

53. Robles-Martinez, P., et al., *3D Printing of a Multi-Layered Polypill Containing Six Drugs Using a Novel Stereolithographic Method.* Pharmaceutics, 2019. **11**(6): p. 274.

54. Bloomquist, C.J., et al., *Controlling release from 3D printed medical devices using CLIP and drug-loaded liquid resins.* Journal of Controlled Release, 2018. **278**: p. 9-23.

55. Kadry, H., et al., *Digital light processing (DLP) 3D-printing technology and photoreactive polymers in fabrication of modified-release tablets.* European Journal of Pharmaceutical Sciences, 2019. **135**: p. 60-67.

56. Trivedi, M.K., et al., *Effect of biofield treatment on spectral properties of paracetamol and piroxicam.* Chemical Sciences Journal, 2015. **6**(3).

57. Krkobabić, M., et al., *Hydrophilic excipients in digital light processing (DLP) printing of sustained release tablets: Impact on internal structure and drug dissolution rate.* International journal of pharmaceutics, 2019. **572**: p. 118790.

58. Kadry, H., et al., *Digital light processing (DLP) 3D-printing technology and photoreactive polymers in fabrication of modified-release tablets.* Eur J Pharm Sci, 2019. **135**: p. 60-67.

59. Green, B.J., et al., *Effect of Molecular Weight and Functionality on Acrylated Poly(caprolactone) for Stereolithography and Biomedical Applications.* Biomacromolecules, 2018. **19**(9): p. 3682-3692.

60. Elbadawi, M., et al., *M3DISEEN: A novel machine learning approach for predicting the 3D printability of medicines.* Int J Pharm, 2020. **590**: p. 119837.

61. Muñiz Castro, B., et al., *Machine learning predicts 3D printing performance of over 900 drug delivery systems.* Journal of Controlled Release, 2021. **337**: p. 530-545.

62. Goh, G.D., S.L. Sing, and W.Y. Yeong, *A review on machine learning in 3D printing: applications, potential, and challenges.* Artificial Intelligence Review, 2021. **54**(1): p. 63-94.

63. Pollard, T.D., et al., *Electrochemical biosensors: a nexus for precision medicine.* Drug Discovery Today, 2021. **26**(1): p. 69-79.

64. Ong, J.J., et al., *Optical biosensors - Illuminating the path to personalized drug dosing.* Biosensors and Bioelectronics, 2021. **188**: p. 113331.

65. Anandakrishnan, N., et al., *Fast Stereolithography Printing of Large‐Scale Biocompatible Hydrogel Models.* Advanced Healthcare Materials, 2021. **10**(10): p. 2002103.

66. Ge, Q., et al., *3D printing of highly stretchable hydrogel with diverse UV curable polymers.* Science advances, 2021. **7**(2): p. eaba4261.

67. Li, W., et al., *A Smartphone‐Enabled Portable Digital Light Processing 3D Printer.* Advanced Materials, 2021. **33**(35): p. 2102153.

68. Wu, D., et al., *3D bioprinting of gellan gum and poly (ethylene glycol) diacrylate based hydrogels to produce human-scale constructs with high-fidelity.* Materials & Design, 2018. **160**: p. 486-495.

69. Li, W., et al., *Recent Advances in Formulating and Processing Biomaterial Inks for Vat Polymerization-Based 3D Printing.* Advanced Healthcare Materials, 2020. **9**(15): p. 2000156.